Case Studies in Chemical and Environmental Engineering 6 (2022) 100260

Contents lists available at ScienceDirect

Case Studies in Chemical and Environmental Engineering

journal homepage: www.sciencedirect.com/journal/case-studies-in-chemical-and-environmental-engineering

Case Report

# Visualization of water accumulation in micro porous layers in polymer electrolyte membrane fuel cells using synchrotron phase contrast tomography

Saad S. Alrwashdeh [a,*], Ala'a M. Al-Falahat [a], Henning Markötter [b,c], Ingo Manke [b]

[a] Mechanical Engineering Department, Faculty of Engineering, Mutah University, P.O Box 7, Al-Karak, 61710, Jordan
[b] Helmholtz-Zentrum Berlin, Hahn-Meitner-Platz 1, 14109, Berlin, Germany
[c] Technische Universität Berlin, Straße des 17. Juni 135, 10623, Berlin, Germany

ARTICLE INFO

*Keywords:*
Polymer electrolyte membrane fuel cell
Microporous layer
Water transport
Synchrotron phase contract tomography

ABSTRACT

Using phase-contracted synchrotron X-ray tomography, this study investigates the water distribution within the microporous layer (MPL) of polymer electrolyte membrane fuel cells (PEMFCs). Synchrotron X-ray tomography used to analyze the water distribution in the whole gas diffusion medium (GDM), which comprises the microporous layer (MPL) and the gas diffusion layer (GDL). The MPL has already been identified. In the future, the development of GDMs could be employed to enhance the performance and operating conditions of PEMFCs.

## 1. Introduction

Due to energy resource scarcity and unequal distribution of it, energy is the most crucial issue of the contemporary period and has become much more prominent recently [1–9]. In order to ensure the energy requirements for various public and industrial life uses, work started on the search for alternative energy sources from this point on [10–14]. This was done as a response to energy challenges in many countries across the world. There are many different alternative energy sources, such as wind and solar power [15–20]. As a fundamental option to guarantee a wide range of transportation uses and energy production for large-scale applications, interest in hydrogen fuel has recently increased. In this situation, fuel cells have emerged as the best way to utilize hydrogen and use it to produce energy for a variety of technical purposes [21–25]. PEMFCs are the most widely utilized forms of fuel cells [26–31]. PEMFCs have a number of technical issues that continue to limit their usage, the most significant of which is the rise in internal water production or the absence of humidity [32–37]. It either limits the chemical reaction from finishing or, on the other hand, reduces the proteins conductivity [38–41].

Due to their zero carbon emissions during operation and their environmental friendliness, fuel cells are regarded as one of the most promising engineering applications for energy generation. Fuel cells have the extra benefit of not having spinning bodies, which lowers their maintenance costs. They also rely on different gases, most notably hydrogen and oxygen, for their cathode and anode electrodes to undergo chemical reactions in order to function [24,27–31]. However, as science and research in this area advance, PEMFCs face some operational issues. The most significant of these is operating at low temperatures, between 50 and 60° Celsius, where they feed water and steam in a manner that hinders the work of the cell and results in issues with channel blockage or lack of brick, as mentioned earlier. From this point on, research was done to address these issues, particularly in operating conditions that depend on previous temperatures [42–45]. Many researchers worked on this, including Alrwashdeh et al., who looked at three different layers for improving the microporous layer: traditional, wavy, and equipped with randomly spaced holes. The randomly dispersed perforated MPL came in second in the performance after the highest efficiency layer which is the wavy layer [24,27–31].

The completion of chemical processes involving several compounds is the basis of fuel cell operation, and the sorts of these chemicals depend on the kind of fuel cell being employed. PEMFCs rely on completing the reaction between hydrogen and oxygen gases, with each gas supplied from one of the fuel cell electrodes to unite these elements. This reaction also produces water as a by-product of the reaction, from which the majority is extracted, as well as an electric current that is used to power various engineering applications. The cell's exterior while preserving another portion to hydrate the cell and aid in its function.

* Corresponding author.
*E-mail address:* saad.alrwashdeh@mutah.edu.jo (S.S. Alrwashdeh).

https://doi.org/10.1016/j.cscee.2022.100260
Received 17 September 2022; Received in revised form 28 September 2022; Accepted 4 October 2022
Available online 4 October 2022

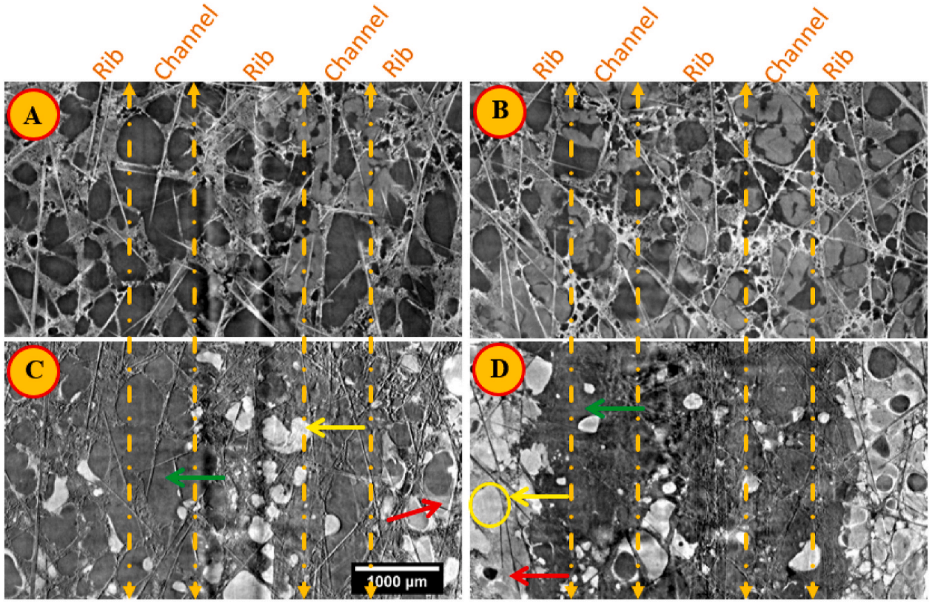


**Fig. 1.** Tomography slices parallel to the membrane through dry anode side (A) as well as cathode side (B), difference between operated and dry state of the anode (C) and the cathode (D).

Following the development of fuel cell technology and the proliferation of studies and research on them, researchers started to get interested in creating their own scientific research methodologies and the means to conduct tests on them. The two most popular techniques are destructive and non-destructive testing, however, non-destructive tests stand out as the best option for learning enough about how cells function and their working circumstances without endangering the cells. Here, it was discovered that the most crucial procedures are ultrasound tests and radiographic methods, which include imaging with neutrons and X-rays. It was noted that each imaging method has a specific use. Due to the great permeability of neutrons and their neutral charge, neutron imaging is one of the key approaches to learning about the inner layers of cells. Due to its low permeability, X-ray imaging is employed for the outer layers; yet, it is regarded as a very dependable instrument for revels a huge amount of information about the surrounding of the fuel cells [46–50]. Because of their superior capacity to detect water molecules, radiographic methods of all sorts are regarded as one of the most efficient approaches to examine the water distribution mechanism inside PEMFCs. The precision of the figures and the difference in resolution when using radiographic techniques to analyze the distribution of water inside fuel cells indicate how the water is distributed both when the fuel cells are operating and when they are not. From this, a comprehensive and precise overview may be obtained in order to undertake a fuel cell improvement in the way that it can function well in future technical applications [51–54].

In order to make its pictures, phase-contrast X-ray imaging gathers data on changes in the phase of an X-ray beam as it travels through an object. Traditional X-ray imaging methods like radiography and computed tomography (CT) rely on the X-ray beam's intensity decreasing (attenuation) as it passes through the sample. This attenuation can be directly measured with the help of an X-ray detector. However, in phase contrast X-ray imaging, the sample's effect on the beam's phase shift isn't observed directly; instead, it's converted into fluctuations in intensity that the detector can subsequently record. Analyzer-based imaging techniques, which reflect the transmitted beam from a Bragg crystal acting as an angular filter, are the second class of phase-contrast imaging strategies that allow for the conversion of refractive effects induced by the object into intensity effects in the detector plane [55–60].

On the basis of old research on mass transport resistance during high current operation, extensive experimental studies have been conducted to comprehend the role of the MPL in water management. By altering MPLs characteristics, such as thickness, porosity, and hydrophobicity, numerical modeling was able to predict liquid water saturation and transport in the GDL, which helped to better understand the inherent behavior of liquid water [61,62].

In this study, the acclamation of the water in the MPL of the PEMFCs is investigated using a synchrotron phase contract tomography.

## 2. Phase contrast tomography

Edge enhancement is applied to phase-contrast images such that the image intensity is no longer solely dependent on the sample's thickness and attenuation. The fringes defining the sample's borders and any internal limits are likely to have both the brightest and lowest brightness in a phase-contrast image. Phase-contrast images may be altered using a process called phase-retrieval to recover the initial phase-shift that the sample imposed on the X-ray wave front in order to retrieve quantitative information from the image.

A reduction in the X-ray beam's intensity as it passes through the sample, which may be observed as a darkening of the beam, is a prerequisite for absorption-based X-ray imaging. Some material compositions, however, simply produce negligible absorption or negligible variations in absorption. Changes in an X-ray beam's phase as it travels through an object are used in phase-contrast imaging. Additionally, the beam's phase shift results in fluctuations in intensity in phase-contrast mode, i.e. at the proper distances, which are captured by the detector.

Phase-contrast imaging, like other phase-contrast techniques, works by having a sample refract X-rays. In order to use X-ray refraction in imaging, particular imaging circumstances are needed since the X-ray refractive index is extremely near to 1, making these refractive effects weaker than the refraction of visible light [63–65].

The X-ray beam is the first prerequisite. The presence of a substantial distance between the sample and the detector is the second important criterion. The Fresnel diffraction fringes in the image are caused by the propagation of the deformed X-ray wave front between the sample and detector after the X-rays have passed through the sample and are distorted in proportion to the phase-shift imposed by the sample.

For phase-contrast imaging, the image generation is controlled by the Fresnel number, with a typical lateral dimension, the wavelength,

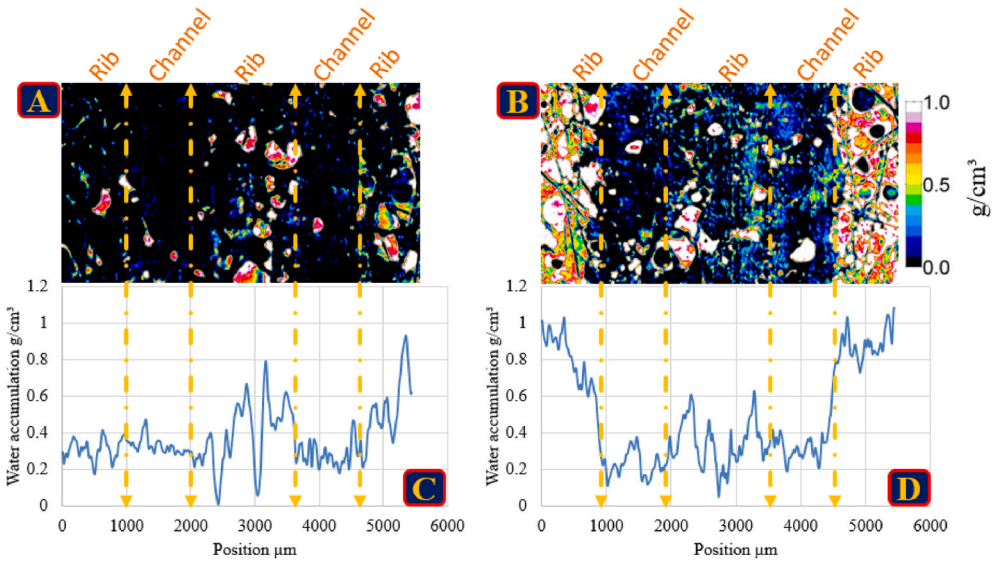


**Fig. 2.** Quantified water density (g/cm$^3$) in the MPL on the anode (A) and on the cathode (B). Water accumulation in the cell at the anode (C) and at the cathode (D).

and the effective propagation distance. Images are in the direct-contrast zone and exhibit noticeable edge enhancement, especially for Fresnel numbers around one. This phenomenon may be explained, for example, using the Transport of Intensity equation (TIE).

As previously indicated, the actual component of the refractive index for visible light can deviate significantly from unity, but the departure from unity for X-rays in various media is often of the order of $10^{-5}$. As a result, the Snell's formula calculation of the refraction angles at the boundary between two isotropic media likewise results in very tiny refraction angles. This has the effect of making it impossible to detect the refraction angles of X-rays passing through tissue samples directly. Instead, they are typically determined indirectly through observation of the interference pattern between diffracted and un diffracted waves caused by spatial variations in the real part of the refractive index.

## 3. Experiment procedure

For this project, a fuel cell that includes SGL 28BCE GDL with MPL and two channels that are 0.5 mm wide and deep on either side was designed. According to the manufacturer, the MPL had a total porosity of roughly 65%. Stoichiometric ratios of 5 were kept on the cathode and anode sides while running the fuel-cell at a current density of 1 A cm$^{-2}$ with an air/hydrogen input.

The tests were carried out at Berlin, Germany's Bessy II electron storage ring's imaging beamline, or "BAMline" [65–67]. A 4008 × 2672 pixel PCO4000 CCD detector was employed. This led to a pixel size of (2.2 × 2.2) µm$^2$ and an associated field of vision of (8.8 × 5.9) mm$^2$ when combined with the used optical system from Optique Peter. For the trials, a beam energy of 19 keV for X-rays was used. There are other places where you may find more information on the measuring method and the instrument utilized.

By selecting a distance of 50 mm between the fuel cell and the detector for the observations zone, it was produced the proper phase contrast. With the use of flat-field photos that contained the plain beam without the cell and dark-field images without the beam, beam transmission was determined by image processing. Before utilizing filtered back projection for volume reconstruction, image filters were applied to the normalized projection pictures. Water is formed as a byproduct of the electrochemical process occurring inside the cell, thus understanding how the water behaves is crucial.

## 4. Result and discussion

Dry slices of the anode (A) and cathode (B) in Fig. 1 are shown parallel to the active layer. The water distribution in the cell is retrieved by subtracting the dry images from the operational images (see Fig. 1(C) and (D)). It should be observed that water encrustations are readily visible in the cell materials' pores. Water agglomerations in the GDL pores are shown by yellow arrows, while dry areas are indicated by green arrows. However, the red arrows in the illustration show that there are also less brilliant patches that may be seen in the MPL water Fig. 1(C) and (D).

By choosing the right attenuation coefficient, the local water density inside the GDM was quantified in Fig. 2. Because water forms on the cathode side, it is seen that the cathode side has a larger water accumulation than the anode side. Due to back diffusion through the membrane and the reduced gas flow in the anode side, water agglomerations develop on the anode side. In addition, due to stronger condensation close to the rib than in channel sections, the water buildup is larger in the rib region than the latter.

The objective of the study was to determine the amounts of water produced by operating the PEMFCs at critical operating conditions, which are within the temperature range of 50–60°. The study was based on examining the quantities of water produced by the operation of the PEMFCs at the temperatures where water droplets are formed and there are no conditions conducive to the formation of water vapor. In order to determine the amount of water that would have resulted from the reaction, the amount of gas that would have been supplied to the cell during operation was calculated, as well as the amount of water that would have left the cell as a result of the chemical reaction, before adding the remaining water to complete the hydration process. The amount of water created within the cell was computed as shown in Fig. 2 with a unit of g/cm$^3$.

## 5. Conclusion

It is demonstrated how the water buildup in the MPL measured using phase contrast synchrotron imaging. It was conduct a three-dimensional investigation of the water buildup. There was far more water detected beneath the ribs than beneath the channels, and there was a distinct boundary dividing the two. The two-phase line that results from local humidity variations in the flowing gases between the rib and channel sections is where we attribute this phenomenon.

The ability to measure local water densities in MPLs offers excellent

prospects for real research on fuel cell materials and may greatly speed up optimization and the adoption of novel MPL designs. This finding might be especially helpful for modeling and simulation as there hasn't been much information available regarding the actual 3D water distribution in MPLs up until now.

## Declaration of competing interest

The authors declare that they have no known competing financial interests or personal relationships that could have appeared to influence the work reported in this paper.

## Data availability

Data will be made available on request.

## References


[1] J. Abu Qadourah, A.M. Alfalahat, S.S. Alrwashdeh, Assessment of solar photovoltaics potential installation into multi-family building's envelope in Amman, Jordan, Cogent Engineering 9 (1) (2022).
[2] J. Abu Qadourah, et al., Improving the energy performance of the typical multi-family buildings in Amman, Jordan, City, Territory and Architecture 9 (1) (2022).
[3] A.M. Al-Falahat, et al., Energy-selective Neutron Imaging by Exploiting Wavelength Gradients of Double Crystal Monochromators—Simulations and Experiments. Nuclear Instruments and Methods in Physics Research, Section A: Accelerators, Spectrometers, Detectors and Associated Equipment, 2019, p. 943.
[4] A.M. Al-Falahat, J.A. Qadourah, S.S. Alrwashdeh, Economic feasibility of heating source conversion of the swimming pools, Journal of Applied Engineering Science 20 (1) (2022) 230–238.
[5] A.M. Al-Falahat, et al., Energy performance and economics assessments of a photovoltaic-heat pump system, Results in Engineering 13 (2022).
[6] S.S. Alrwashdeh, Determining the optimum tilt solar angle of a PV applications at different sites in Jordan, J. Eng. Appl. Sci. 12 (Specialissue11) (2017) 9295–9303.
[7] S.S. Alrwashdeh, Predicting of energy production of solar tower based on the study of the cosine efficiency and the field layout of heliostats, Int. J. Mech. Eng. Technol. 9 (11) (2018) 250–257.
[8] S.S. Alrwashdeh, Investigation of the energy output from PV racks based on using different tracking systems in Amman-Jordan, Int. J. Mech. Eng. Technol. 9 (10) (2018) 687–694.
[9] S.S. Alrwashdeh, Comparison among solar panel arrays production with a different operating temperatures in Amman-Jordan, Int. J. Mech. Eng. Technol. 9 (6) (2018) 420–429.
[10] S.S. Alrwashdeh, Energy production evaluation from a linear fresnel reflectors arrays with different array orientation, Int. J. Eng. Res. Technol. 11 (11) (2018) 1811–1819.
[11] S.S. Alrwashdeh, Assessment of the energy production from PV racks based on using different solar canopy form factors in Amman-Jordan, Int. J. Eng. Res. Technol. 11 (10) (2018) 1595–1603.
[12] S.S. Alrwashdeh, The effect of solar tower height on its energy output at Ma'an-Jordan, AIMS Energy 6 (6) (2018) 959–966.
[13] S.S. Alrwashdeh, Modelling of operating conditions of conduction heat transfer mode using energy 2D simulation, International Journal of Online Engineering 14 (9) (2018) 200–207.
[14] S.S. Alrwashdeh, Assessment of photovoltaic energy production at different locations in Jordan, Int. J. Renew. Energy Resour. 8 (2) (2018) 797–804.
[15] S.S. Alrwashdeh, An energy production evaluation from PV arrays with different inter-row distances, Int. J. Mech. Prod. Eng. Res. Dev. 9 (5) (2019) 1–10.
[16] S.S. Alrwashdeh, Energy production assessment of solar tower based on the study of the mirror shadowing and blocking effects, Universal Journal of Mechanical Engineering 7 (2) (2019) 71–76.
[17] S.S. Alrwashdeh, Investigation of wind energy production at different sites in Jordan using the site effectiveness method, Energy Eng. J. Assoc. Energy Eng.: Journal of the Association of Energy Engineering 116 (1) (2019) 47–59.
[18] S.S. Alrwashdeh, Investigation of the energy output from PV panels based on using different orientation systems in Amman-Jordan, Case Stud. Therm. Eng. 28 (2021).
[19] S.S. Alrwashdeh, Investigation of the energy output of parabolic trough racks based on using different rhomboid layout, ARPN Journal of Engineering and Applied Sciences 17 (5) (2022) 578–586.
[20] S.S. Alrwashdeh, Energy sources assessment in Jordan, Results in Engineering 13 (2022).
[21] S.S. Alrwashdeh, Investigation of the effect of the injection pressure on the direct-ignition diesel engine performance, AIMS Energy 10 (2) (2022) 340–355.
[22] S.S. Alrwashdeh, A.M. Al-Falahat, T.K. Murtadha, Effect of turbocharger compression ratio on performance of the spark-ignition internal combustion engine, Emerging Science Journal 6 (3) (2022) 482–492.
[23] S.S. Alrwashdeh, F.M. Alsaraireh, Wind energy production assessment at different sites in Jordan using probability distribution functions, ARPN Journal of Engineering and Applied Sciences 13 (20) (2018) 8163–8172.
[24] S.S. Alrwashdeh, et al., In-situ investigation of water distribution in polymer electrolyte membrane fuel cells using high-resolution neutron tomography with 6.5 μm pixel size, AIMS Energy 6 (4) (2018) 607–614.
[25] S.S. Alrwashdeh, H. Ammari, Life cycle cost analysis of two different refrigeration systems powered by solar energy, Case Stud. Therm. Eng. 16 (2019).
[26] S.S. Alrwashdeh, et al., The effect of heat exchanger design on heat transfer rate and temperature distribution, Emerging Science Journal 6 (1) (2022) 128–137.
[27] S.S. Alrwashdeh, et al., Improved performance of polymer electrolyte membrane fuel cells with modified microporous layer structures, Energy Technol. 5 (9) (2017) 1612–1618.
[28] S.S. Alrwashdeh, et al., Neutron radiographic in operando investigation of water transport in polymer electrolyte membrane fuel cells with channel barriers, Energy Convers. Manag. 148 (2017) 604–610.
[29] S.S. Alrwashdeh, et al., *In* operando quantification of three-dimensional water distribution in nanoporous carbon-based layers in polymer electrolyte membrane fuel cells, ACS Nano 11 (6) (2017) 5944–5949.
[30] S.S. Alrwashdeh, et al., Investigation of water transport dynamics in polymer electrolyte membrane fuel cells based on high porous micro porous layers, Energy 102 (2016) 161–165.
[31] S.S. Alrwashdeh, et al., X-ray tomographic investigation of water distribution in polymer electrolyte membrane fuel cells with different gas diffusion media, in: Joint General Session: Batteries and Energy Storage -and- Fuel Cells, Electrolytes, and Energy Conversion - 229th ECS Meeting, Electrochemical Society Inc, 2016.
[32] S.S. Alrwashdeh, J.A. Qadourah, A.M. Al-Falahat, Investigation of the effect of roof color on the energy use of a selected house in amman, Jordan, Front. Mech. Eng. 8 (2022).
[33] O.R. Altarawneh, et al., Energy and exergy analyses for a combined cycle power plant in Jordan, Case Stud. Therm. Eng. (2022) 31.
[34] H.D. Ammari, S.S. Al-Rwashdeh, M.I. Al-Najideen, Evaluation of wind energy potential and electricity generation at five locations in Jordan, Sustain. Cities Soc. 15 (2015) 135–143.
[35] M. Göbel, et al., Transient limiting current measurements for characterization of gas diffusion layers, J. Power Sources 402 (2018) 237–245.
[36] Y.S. Jweihan, et al., Improvements to the duplicate shear test (DST) device for measuring the fundamental shear properties of asphalt concrete mixes, International Journal of Pavement Research and Technology (2022).
[37] H. Markötter, et al., Morphology correction technique for tomographic in-situ and operando studies in energy research, J. Power Sources 414 (2019) 8–12.
[38] T.K. Murtadha, et al., Improving the cooling performance of photovoltaic panels by using two passes circulation of titanium dioxide nanofluid, Case Stud. Therm. Eng. 36 (2022).
[39] J.A. Qadourah, A.M. Al-Falahat, S.S. Alrwashdeh, Investigate the carbon footprints of three intermediate flooring systems: cross-laminated timber, solid concrete, and hollow-core precast concrete, Journal of Applied Engineering Science 20 (2) (2022) 377–385.
[40] M.A. Saraireh, F.M. Alsaraireh, S.S. Alrwashdeh, Investigation of heat transfer for staggered and in-line tubes, Int. J. Mech. Eng. Technol. 8 (11) (2017) 476–483.
[41] F. Sun, et al., Complementary X-ray and neutron radiography study of the initial lithiation process in lithium-ion batteries containing silicon electrodes, Appl. Surf. Sci. 399 (2017) 359–366.
[42] F. Duan, et al., Model parameters identification of the PEMFCs using an improved design of Crow Search Algorithm, Int. J. Hydrogen Energy (2022).
[43] Z. Huang, Q. Jian, Cooling efficiency optimization on air-cooling PEMFC stack with thin vapor chambers, Appl. Therm. Eng. 217 (2022), 119238.
[44] X. Chen, et al., Performance evaluation on thermodynamics-economy-environment of PEMFC vehicle power system under dynamic condition, Energy Convers. Manag. 269 (2022), 116082.
[45] T. Meng, et al., Optimization and efficiency analysis of methanol SOFC-PEMFC hybrid system, Int. J. Hydrogen Energy 47 (64) (2022) 27690–27702.
[46] S. Pollastri, et al., Characterization of innovative Pt-ceria catalysts for PEMFC by means of ex-situ and operando X-Ray Absorption Spectroscopy, Int. J. Hydrogen Energy 47 (14) (2022) 8799–8810.
[47] T. Sasabe, S. Tsushima, S. Hirai, In-situ visualization of liquid water in an operating PEMFC by soft X-ray radiography, Int. J. Hydrogen Energy 35 (20) (2010) 11119–11128.
[48] P. Deevanhxay, et al., Investigation of water accumulation and discharge behaviors with variation of current density in PEMFC by high-resolution soft X-ray radiography, Int. J. Hydrogen Energy 36 (17) (2011) 10901–10907.
[49] P. Deevanhxay, et al., In situ diagnostic of liquid water distribution in cathode catalyst layer in an operating PEMFC by high-resolution soft X-ray radiography, Electrochem. Commun. 22 (2012) 33–36.
[50] J. Kim, et al., Breakthrough/drainage pressures and X-ray water visualization in gas diffusion layer of PEMFC, Curr. Appl. Phys. 12 (1) (2012) 105–108.
[51] T. Nojima, et al., Development of an imaging system for the observation of water behavior in a channel in PEMFC, Phys. Procedia 43 (2013) 282–287.
[52] Z. Yu, et al., Improvement of the three-dimensional fine-mesh flow field of proton exchange membrane fuel cell (PEMFC) using CFD modeling, artificial neural network and genetic algorithm, Int. J. Hydrogen Energy (2022).
[53] Y. Li, et al., Effects of surfactant CTAB on performance of flat-plate CLPHP based on PEMFC cooling, Int. J. Heat Mass Tran. 196 (2022), 123226.
[54] F.C. Lee, et al., Alternative architectures and materials for PEMFC gas diffusion layers: a review and outlook, Renew. Sustain. Energy Rev. 166 (2022), 112640.
[55] Y. Liu, Z. Tu, S.H. Chan, Performance enhancement in a H2/O2 PEMFC with dual-ejector recirculation, Int. J. Hydrogen Energy 47 (25) (2022) 12698–12710.
[56] D. A R, D. Ganguly, R. Sundara, High temperature annealed (002) oriented WO3 nanoplatelets with uniform Pt decoration as durable carbon free anode

electrocatalyst for PEMFC application, Int. J. Hydrogen Energy 47 (59) (2022) 24978–24990.
[57] H. Pourrahmani, et al., Progress in the proton exchange membrane fuel cells (PEMFCs) water/thermal management: from theory to the current challenges and real-time fault diagnosis methods, Energy Rev. 1 (1) (2022), 100002.
[58] J. Jia, et al., Designing independent water transport channels to improve water flooding in ultra-thin nanoporous film cathodes for PEMFCs, Int. J. Hydrogen Energy 47 (49) (2022) 21261–21272.
[59] J. Bedet, et al., Magnetic resonance imaging of water distribution and production in a 6cm2 PEMFC under operation, Int. J. Hydrogen Energy 33 (12) (2008) 3146–3149.
[60] Q. Liu, et al., Polyethyleneimine-filled sepiolite nanorods-embedded poly(2,5-benzimidazole) composite membranes for wide-temperature PEMFCs, J. Clean. Prod. 359 (2022), 131977.
[61] G. Ouaidat, et al., Study of the effect of mechanical uncertainties parameters on performance of PEMFC by coupling a 3D numerical multiphysics model and design of experiment, Int. J. Hydrogen Energy 47 (56) (2022) 23772–23786.
[62] A. Iranzo, et al., Water build-up and evolution during the start-up of a PEMFC: visualization by means of Neutron Imaging, Int. J. Hydrogen Energy 42 (19) (2017) 13839–13849.
[63] Y. Wu, et al., Enhanced phase retrieval via deep concatenation networks for in-line X-ray phase contrast imaging, Phys. Med. 95 (2022) 41–49.
[64] Y. Xu, et al., Single-shot grating-based X-ray phase contrast imaging via generative adversarial network, Opt Laser. Eng. 152 (2022), 106960.
[65] R.A. Herring, Diffracted beam interferometry – differential phase contrast image of an amorphous thin film material, Micron 160 (2022), 103317.
[66] M.F. Guerra, et al., Analysis of trace elements in gold alloys by SR-XRF at high energy at the BAMline, Nucl. Instrum. Methods Phys. Res. Sect. B Beam Interact. Mater. Atoms 266 (10) (2008) 2334–2338.
[67] A. Rack, et al., High resolution synchrotron-based radiography and tomography using hard X-rays at the BAMline (BESSY II), Nucl. Instrum. Methods Phys. Res. Sect. A Accel. Spectrom. Detect. Assoc. Equip. 586 (2) (2008) 327–344.